

Dynamics of Homogeneous Charge Compression Ignition (HCCI) Engines with High Dilution

C. J. Chiang and A. G. Stefanopoulou
University of Michigan, Ann Arbor
Email: cjchiang,annastef@umich.edu

Abstract—This paper analyzes the stability of the autoignition process of homogeneous charge compression ignition (HCCI) engines in light of the cycle-to-cycle thermal feedback due to the high percentage of exhaust dilution. The influence of heat transfer and the cooling system on the system stability is investigated. The returning map and the stability of the multiple steady state equilibria are confirmed with a high order dynamic nonlinear model, which includes manifold filling and composition dynamics and has been validated both at steady state and during transient. It is shown that the autoignition, which is based on high exhaust gas recirculation and thus strong cycle-to-cycle temperature coupling, can depart from the region of attraction of a stable equilibrium during large and fast changes in fueling level.

I. INTRODUCTION

Charge temperature is the primary mechanism for controlling ignition timing in an HCCI engine, especially when exhaust gas recirculation (EGR) is used [1], [2], [3]. The recirculation of hot exhaust gas provides high dilution and thus changes the charge temperature inside the cylinder [4], [5]. One attractive way to recirculate the hot exhaust gas involves a secondary opening of the exhaust valve during the intake stroke (rebreathing). The amount of dilution is controlled by varying the lift of the secondary exhaust valve opening, which we refer to as the rebreathing lift (RBL), as shown in the valve profiles in Fig. 1. Using high dilution levels the exhaust gas heat can increase the charge temperature for the next cycle, and thus determine the ignition and the exhaust temperature of the subsequent cycle [6], [7]. Therefore, thermal autoignition equilibria and their stability can be described by a returning map that captures the temperature effect of the prior combustion to the next via the exhaust gas recirculation [8].

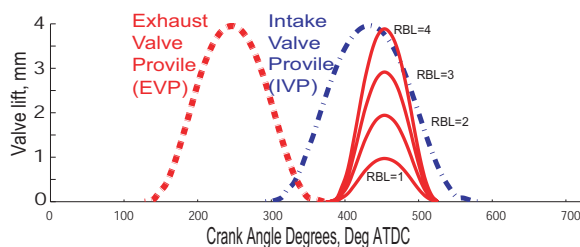


Fig. 1. Exhaust, intake and rebreathing valve profiles.

In this paper, we extend the model in [6] and the stability analysis in [8] for an HCCI engine with high dilution by

exploring the effect of heat transfer in the exhaust runners. The modified model is first validated against transient experiments and then used to analyze the effect of heat transfer in the exhaust runners on the open loop stability of a HCCI engine by building the returning map following a procedure similar to [8]. By assuming fast manifold dynamics and accurate air-to-fuel ratio control, the temperature dynamics constitute the dominant and slow dynamics of the overall system. Specifically, the charge temperature in the cylinder at intake valve closing, T_{ivc} , and the blow down temperature, T_{bd} , are the two cycle-to-cycle interacting variables that define the HCCI combustion process. The cycle-to-cycle coupling of the temperature dynamics thus determines the stability of the open loop HCCI dynamics.

We found that the thermal dynamics are described by a unique stable thermal equilibrium, if the wall temperature (T_w) of the exhaust runners and exhaust manifold are perfectly controlled with an active cooling system. On the other hand, insulated exhaust runners sustain the thermal energy of the recycled gases and may enhance cycle-to-cycle temperature growth under early-ignition conditions, as explained in this paper and observed in the experiments [9], [2]. In the end, we demonstrate that non-optimized sequences of the input command RBL, which successfully make small load transitions, can result in large temperature excursions that can damage the engine or lead to misfire during large load transitions.

II. ENGINE MODEL

A summary of the HCCI engine model dynamics is presented in this section. The mean value model (MVM) from [6] is extended by accounting for the heat losses in the exhaust runners. This extension allows us to study the effect of heat transfer on the multiplicity and stability of the temperature equilibria. Figure 2 shows the schematic diagram associated with the engine model. There are three relevant volumes: (i) the intake manifold denoted with subscript 1, (ii) the exhaust manifold denoted with subscript 2, and (iii) the cylinder denoted with subscript c. The atmospheric conditions are denoted with subscript 0. In each volume, volumes are denoted with V, pressures with p, temperatures with T, masses with m. The rate of the flow from volume x to volume y is denoted as W_{xy} and is calculated based on the orifice flow equation [10].

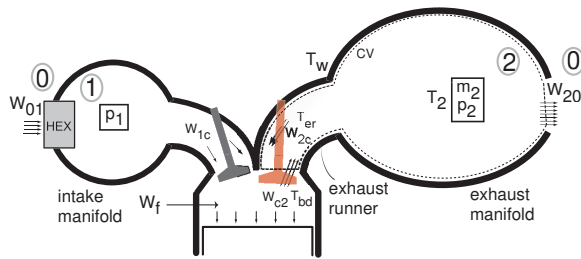


Fig. 2. Schematic diagram of the engine.

A. System Dynamics

The burned gas compositions are neglected in this model since the combustion timing of a high residual HCCI engine is dominated by charge temperature [1], [2], [3]. The system dynamics include three (3) continuous and two (2) discrete in-time states. A heat exchanger (HEX) keeps the intake manifold at isothermal conditions, $T_1 = 90^\circ\text{C}$ (363°K). Therefore, one continuous state is sufficient to characterize the intake manifold, namely, the spatially average intake manifold pressure, p_1 , which is determined through the conservation of the mass in the intake manifold and the ideal gas law:

$$\dot{p}_1 = RT_1 (W_{01} - W_{1c}) / V_1 \quad (1)$$

where R is the gas constant. For most conditions, the manifold pressures satisfy $p_1 < p_0 < p_2$ so that all the flows through the valves and orifices are due to the pressure difference between the volumes. The flow from the intake manifold to the cylinder W_{1c} is a forced flow due to cylinder pumping and has been characterized in [6] using experimental data as a function of p_1 , p_2 and the rebreathing lift (RBL). Similarly, the rebreathing flow W_{2c} has been characterized in [6] as a function of p_1 , p_2 , RBL, and the exhaust runner temperature T_{er} discussed below.

The two other continuous states are in the exhaust manifold. One of them is given by the conservation of mass in the control volume containing the whole space of exhaust manifold plus runners (CV in Fig. 2):

$$\dot{m}_2 = W_{c2} - W_{20} - W_{2c}. \quad (2)$$

The energy balance equation in the control volume CV includes the heat transfer to the wall by defining the convective area A_2 and the convection coefficient h_2 ($A_2 h_2 = 3 \text{ W/K}$). A perfect cooling system is assumed and thus the temperature of wall T_w surrounding the exhaust runners and manifold is assumed constant at 400°K . The conservation of energy gives the final continuous state:

$$\frac{d}{dt} p_2 = \frac{\gamma R}{V_2} \left(W_{c2} T_{bd}^d - (W_{20} + W_{2c} + W_{21}) T_2 \right) - \frac{A_2 h_2 R}{C_v V_2} (T_2 - T_w) \quad (3)$$

where V_2 is the volume of the exhaust manifold plus runners (CV) and T_{bd}^d is the delayed temperature of the blowdown gas entering the exhaust runners as introduced in (5).

Two discrete-in-time states are introduced due to the cycle-delay $\tau = N/120$, where N is the engine speed (rev/min). Specifically, the flow and temperature of the gas exiting the

cylinder are both delayed:

$$W_{c2}(t + \tau) = W_{1c}(t) + W_f(t) + W_{2c}(t) \quad (4)$$

$$T_{bd}^d(t + \tau) = T_{bd}(t) \quad (5)$$

where W_f is the fuel mass flow injected, and T_{bd} is the temperature of the blowdown gas in the previous cycle. The blowdown gas temperature T_{bd} is calculated in the combustion model in Sec. II-B.

The temperature of the reinducted exhaust gas, T_{er} , is derived by (i) considering the period right after the exhaust valve closing (EVC) in the energy balance equation of the exhaust runners and (ii) integrating the resulting energy balance equation from EVC ($t = 0$) to middle of the intake stroke ($t = t_r$):

$$T_{er} = \frac{T_w T_{bd}^d}{(1 - \alpha_{ht}) T_{bd}^d + \alpha_{ht} T_w} \quad (6)$$

where $\alpha_{ht} = \exp\left(\frac{-4h_{er}RT_w t_r}{C_v D_{er} p_2}\right)$

The parameter D_{er} is the effective diameter of the exhaust runner and h_{er} is the heat transfer coefficient in the exhaust runner. The ratio α_{ht} weighs the heat gained from the blowdown gases versus the heat lost to the wall.

B. Combustion ($T_{ivc} \rightarrow T_{bd}$)

The combustion model in [6] is summarized in this section. The blowdown temperature T_{bd} is derived by tracing the temperature variations through the following process: compression from intake valve closing (IVC), combustion, expansion and blowdown.

$$T_{bd} = T_{ivc} \left(\frac{p_2}{p_{ivc}} \right)^{1 - \frac{1}{\gamma_e}} \left[\left(\frac{V_c(\theta_c)}{V_{ivc}} \right)^{n_e - n_c} + \frac{V_c^{n_e - 1}(\theta_c) R Q_{LHV} m_f}{C_v V_{ivc}^{n_e} p_{ivc}} \right]^{\frac{1}{n_e}} \quad (7)$$

where m_f is the amount of fuel injected per cycle and θ_c denotes the end of combustion

$$\theta_c = \theta_{soc} + \Delta\theta. \quad (8)$$

The start of combustion θ_{soc} is determined by the Arrhenius integral:

$$\int_{\theta_{ivc}}^{\theta_{soc}} A p_{ivc}^n v_{ivc}^{n_c n}(\vartheta) \exp\left(-\frac{E_a v_{ivc}^{1-n_c}(\vartheta)}{RT_{ivc}}\right) d\vartheta = 1 \quad (9)$$

where $v_x(\vartheta_y) = V_c(\vartheta_x) / V_c(\vartheta_y)$

and the combustion duration $\Delta\theta$ in (8) is calculated by a reparameterized burning velocity equation:

$$\Delta\theta = k (T_{soc})^{(-2/3)} (T_m)^{1/3} \exp\left(\frac{E_c}{3R_u T_m}\right) \quad (10)$$

where $T_m = T_{soc} + e\Delta T$, $\Delta T = Q_{LHV} m_f / C_v m_c$
 $e = b_0 + b_1 \theta_{soc} + b_2 \theta_{soc}^2$.

Integration of (7)-(10) results in the overall combustion model that relates T_{bd} to the combustion model inputs T_{ivc} , p_1 , p_2 and m_f

$$T_{bd} = f_c(T_{ivc}, p_1, p_2, m_f). \quad (11)$$

The dependency of T_{bd} on T_{ivc} , which in turn depends on the previous T_{bd} , constitutes the feedback loop, shown in Fig. 3, that we analyze in this paper.

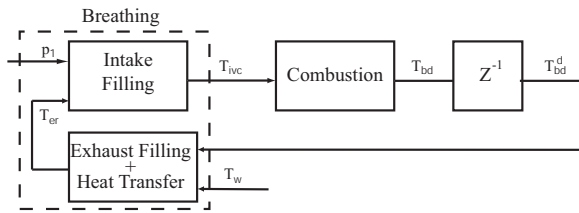


Fig. 3. The thermal feedback constituted by the breathing characteristics (including heat transfer in the exhaust runners and exhaust manifold) and the combustion characteristics of the HCCI engine with large percentage of residual gas in the cylinder charge.

C. Breathing ($T_{bd} \rightarrow T_{er} \rightarrow T_{ivc}$)

In this section, we construct the steady state characteristics of the breathing block in Fig. 3, which maps the blowdown temperature T_{bd} to intake charge temperature T_{ivc} through the reinducted exhaust temperature T_{er} . The steady state temperature at IVC, T_{ivc} , is derived in [8] as

$$T_{ivc} = \frac{(\beta_0 + \beta_1 p_1) V_{ivc} T_{er}}{W_{01} \tau R (T_{er} - T_1) + (\beta_0 + \beta_1 p_1) V_{ivc}}. \quad (12)$$

At steady-state, based on (2), (3), and (5), exhaust manifold temperature T_2 is a weighted function of the blowdown temperature T_{bd} and the wall temperature T_w :

$$T_2 = \frac{C_p W_{c2} T_{bd} + A_2 h_2 T_w}{C_p W_{c2} + A_2 h_2}. \quad (13)$$

The temperature of the reinducted exhaust gas T_{er} at steady state is derived from (5) and (6):

$$T_{er} = \frac{T_w T_{bd}}{(1 - \alpha_{ht}) T_{bd} + \alpha_{ht} T_w} \quad (14)$$

where $\alpha_{ht} = \exp\left(\frac{-4h_{er}RT_w}{C_v D_{er} p_2} t_r\right)$.

The ratio α_{ht} weighs the heat gained from the blowdown gases versus the heat lost to the wall. If there is no heat loss to the wall as in insulated exhaust runners, then $\alpha_{ht} = 1$ and $T_{er} = T_{bd}$. In all other cases, $\alpha_{ht} < 1$, which weakens the thermal coupling ($T_{bd} \rightarrow T_{er} \rightarrow T_{ivc} \rightarrow \text{new } T_{bd}$) from cycle-to-cycle.

Typical values of the parameters can be used to illustrate how heat transfer affects the slope of the breathing temperature curve. For example, by using $h_{er} = 80 \text{ W/m}^2\text{K}$, $C_v = 740.625 \text{ kJ/kg}\cdot^\circ\text{K}$, $p_2 = 102.06 \text{ kPa}$ and $T_w = 400^\circ\text{K}$ in equation (14), the temperature of the reinducted exhaust gas is approximately

$$T_{er} \approx 0.8 T_{bd}. \quad (15)$$

Compared with the case when the exhaust runners are insulated, $T_{er} = T_{bd}$, the resulting steady state slope from T_{bd} to T_{er} in (15) is reduced by 20%. Thus by substituting (15) into (12), the slope of the steady state temperature curve from T_{bd} to T_{ivc} is also reduced. Specifically, the steady state gain from T_{bd} to T_{ivc} decreases when a higher heat transfer rate is applied (increased h_{er}).

III. TRANSIENT TREND VALIDATION

Experimental data during step changes in RBL and fuel (independently) for a single-cylinder gasoline HCCI engine were provided for validation by General Motors Co after the engine was modified from the original engine that was used to develop the model. Due to the differences between the engines used for model calibration versus validation, an offset between the experiment and simulation is observed. To facilitate the comparison between the predicted and the measured values and demonstrate that the dynamic model captures the transient cycle-to-cycle behavior, two vertical axes will be used for the validation figures in this section. The left axis shows the measured values, whereas the right axis shows the predicted values.

The validation data were provided at a fixed rate with 0.05 sec sampling time after downsampling from a sampling time of 0.005 sec. Hence, at 1000 RPM, the values of the crank angle of 50% fuel burned (θ_{CA50}) values capture cycle-to-cycle variability. The two experiments were performed in two different periods. The exhaust runner temperature measurement is important for validating and unraveling the thermal coupling by the rebreathed flow. For the validation, we augment associated sensor dynamics in the reinducted gas temperature T_{er} of our model to compare with the measured temperature T_{meas} . A slow thermocouple with time constant 10.68 sec (89 cycles at 1000 RMP) was used for the exhaust runner temperature during the RBL steps. The experiment with the fuel steps was performed with a faster thermocouple at the exhaust runner with time constant 1.2 sec (10 cycles at 1000 RPM).

The transient response during RBL steps and fuel steps are shown in Fig. 4 and Fig. 5. The figures show that θ_{CA50} is advanced when either RBL or fuel increases. The measured temperature at the exhaust runner, T_{meas} , is the reinducted exhaust gas temperature, T_{er} , modified by the sensor dynamics. The absence of wall temperature dynamics in the model induces the mismatch between the modeled T_{er} and the measure T_{meas} in Fig. 5. Fig. 4 shows that the measured temperature T_{meas} increases more in the second RBL step change (from 3 mm to 4 mm) than in the first one (from 2 mm to 3 mm). This nonlinear behavior between RBL and T_{meas} (T_{er}) is predicted by our combustion model. Specifically, the reinducted exhaust gas temperature T_{er} (6) depends on the nonmonotonic behavior of T_{bd} as T_{ivc} is increased through RBL. The implication of this nonlinear behavior to the thermal stability of an HCCI engine was first reported in [8] and is further studied in this paper.

IV. GLOBAL STEADY-STATE TEMPERATURE EQUILIBRIA

Assuming that the temperature dynamics dominate the engine behavior, we analyze the global temperature equilibria using a return map consisting of two processes, namely: the combustion process in Sec. II-B and the breathing process in Sec. II-C. The internal temperature feedback shown schematically in Fig. 3 exists in a small percentage in conventional SI or CI engines, but its effects are pronounced in HCCI

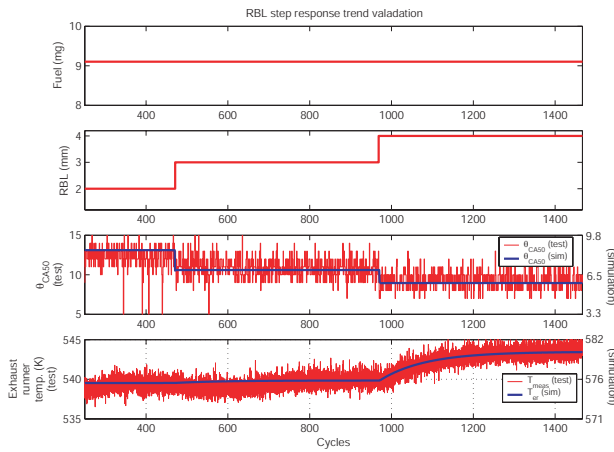


Fig. 4. Rebreathing lift step response trend validation.

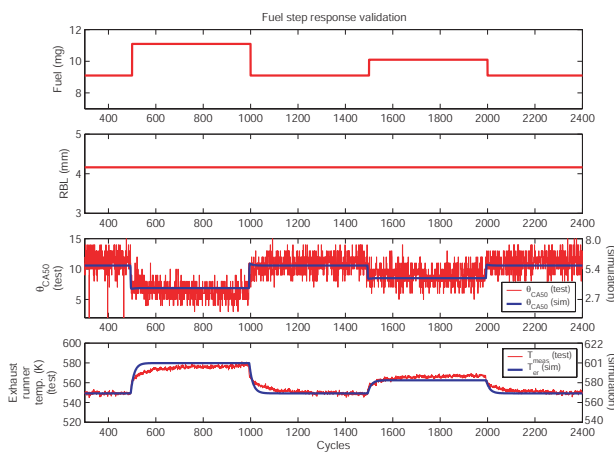


Fig. 5. Fuel step response trend validation.

engines due to the large percentage of residual gas in the cylinder charge.

To get the exact mapping from T_{bd} to T_{ivc} (breathing) and from T_{ivc} to T_{bd} (combustion), the exact manifold pressures need to be determined for fixed fueling and RBL. To resolve the coupling, the steady state equations are programmed and solved using the symbolic manipulations in Matlab. Specifically, the temperature equations used are:

- Eq. (11) for $T_{bd} = f_c(T_{ivc}, p_1, p_2, W_f)$
- Eq. (14) for $T_{er} = f_{b1}(T_{bd}, p_2)$;
- Eq. (12) for $T_{ivc} = f_{b2}(T_{er}, p_1)$;
- Eq. (13) for $T_2 = f_{b3}(T_{bd}, p_1, p_2, RBL)$;

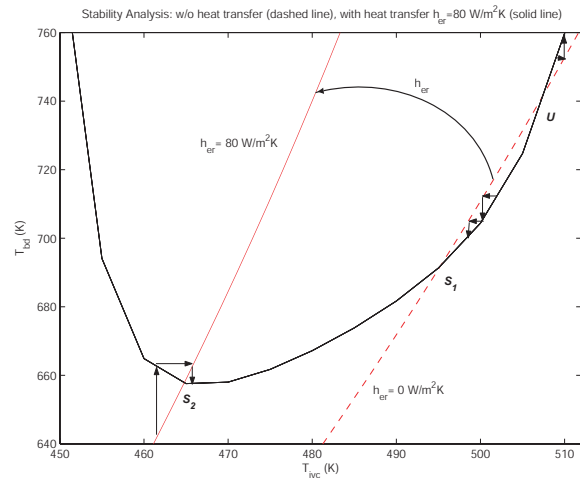
and mass flow rate equations are

- $W_{1c}(p_1, p_2, RBL) = W_{01}(p_1)$
- $W_{20}(p_2, T_2) = W_{01}(p_1) + W_f$
- $W_{c2} = W_{01}(p_1) + W_{2c}(p_1, p_2, T_{rbl}, RBL) + W_f$.

Note here that the flows depend on the temperatures and so the steady-state temperature and flow equations need to be solved simultaneously.

To obtain a graphical representation of the HCCI engine temperature equilibria, in Fig. 6 we superimpose the breath-

ing temperature curves (straight lines) together with the combustion temperature curve (“U” shape), for a fixed fuel flow rate at 9 mg/cycle, RBL at 4 mm and intake manifold pressure p_1 at 100.19 kPa. The breathing temperature curves (straight lines in Fig. 6) provide the cylinder charge temperature at IVC of the next cycle, $T_{ivc}(k+1) = f_b(T_{bd}(k))$, as it is governed by the breathing characteristics under different heat transfer conditions. The addition of heat transfer in the exhaust runners ($h_{er} = 80 \text{ W}^2/\text{K}$) changes the slope of the curve, a change which is critical to the steady-state mapping. The combustion temperature curve (“U” shape in Fig. 6) provides the blowdown temperature of cycle k , $T_{bd}(k) = f_c(T_{ivc}(k))$, as it is governed by the combustion following the autoignition of the compressed charge. It is obvious from Fig. 6 that there is a fuel-optimum T_{ivc}^* on the combustion curve for which most of the chemical energy of the fuel is converted to useful mechanical work and not exhaust gas heat. In other words, T_{ivc} determines combustion timing in the HCCI engine and thus affects the thermal efficiency. The intersection of the breathing curve (straight line) and the combustion curve (“U” shape) defines a temperature equilibrium point.

Fig. 6. Stability analysis through the recursive mapping between T_{ivc} and T_{bd} for fuel flow rate fixed at 9 mg/cycle.

The stability of an equilibrium point for the recursive mapping is determined by the slopes of the two curves near the intersection. We conclude that stable equilibria exist when $|\frac{\partial T_{bd}}{\partial T_{ivc}} \frac{\partial T_{ivc}}{\partial T_{bd}}| < 1$. Basically, the equilibrium is stable around the lowest point on the combustion curve (T_{bd} at 660°K; T_{ivc} at 465°K). On the other hand, unstable equilibrium points appear when the two curves have two intersections, as with the dotted line in the right portion of Fig. 6. This dotted line corresponds to the breathing characteristics of an engine with insulated exhaust runners ($h_{er} = 0 \text{ W}/\text{m}^2\text{K}$). When RBL is 4 mm and p_1 is equal to 100.19 kPa, one of the intersections of the breathing and combustion curves is a stable equilibrium point. The stability of this equilibrium can be confirmed by following the temperature converging sequence after a small perturbation from the equilibrium point, S_1 , as shown in

Fig. 6. The other intersection, point U in Fig. 6, is an unstable equilibrium point. With the addition of heat transfer in the exhaust runners ($h_{er} = 80 \text{ W/m}^2\text{K}$), the slope of the breathing temperature curve (from T_{bd} to T_{ivc}) increases as shown in Fig. 6. This slope change corresponds to a weaker cycle-to-cycle coupling of the temperature dynamics. Extremely high heat transfer case (high h_{er}) would result in a vertical breathing temperature curve and stop the internal feedback loop from T_{bd} to T_{ivc} . Specifically, extremely high h_{er} implies $\alpha_{ht} \rightarrow 0$ and $T_{er} \rightarrow T_w$ as indicated by (14). In other words, T_{ivc} is only affected by the wall temperature T_w from (12). We conclude that the wall temperature and heat management are very important to the operation of HCCI engines.

With better understanding of the heat transfer effect on the stability of HCCI engine, we can develop a better heat management strategy to provide enough heat required for autoignition and avoid instability. For instance, a controllable and fully integrated cooling system could be used to enhance the self-heating tendency at some operating points for fast warm-up strategies. On the other hand, we may have to cool down the exhaust runners to avoid instability or early ignition at high loads.

V. CONTROLLED TEMPERATURE TRAJECTORIES

To generate the simple two dimensional returning maps in Sec. IV we neglected the intake and exhaust manifold filling dynamics and assumed that the equilibrium flow is achieved much faster than the equilibrium temperature. In this section, we use the full order model in [6] to illustrate transitions between the identified temperature equilibria during critical load transitions. The unmeasurable T_{bd} on the y-axis of the steady-state temperature map in Fig. 6 can be replaced with the measurement T_{er} by augmenting (14). A moderate heat transfer coefficient $h_{er} = 60 \text{ W/m}^2\text{K}$ is picked to generate both the steady-state (T_{ivc}, T_{er}) map and the temperature trajectories. We demonstrate that a static feedforward controller and the dynamic feedforward controller in [11], both of which successfully make small load transitions, can result in large temperature excursions that can damage the engine or lead to misfire during large load transitions.

The dynamic feedforward controller in [11] is summarized as follows. Fig. 7 shows the linearized HCCI engine plant with a dynamic (cancellation) feedforward controller and an integral feedback controller. The HCCI engine plant is linearized around the equilibrium point of 9 mg/cycle fueling rate and 3.6 mm RBL. The input-output behavior of the linearized plant can thus be represented by the transfer functions from Fuel and RBL to the combustion timing CA_{50} (crankangle for 50% fuel burned):

$$CA_{50} = G_{yw} \cdot Fuel + G_{yu} \cdot RBL. \quad (16)$$

A cancellation feedforward controller from Fuel to RBL can be derived from the transfer functions G_{yw} and G_{yu} [11]:

$$C_{uw} = -G_{yu}^{-1} G_{yw}. \quad (17)$$

In practice, the plant transfer functions can be derived from a real-time identification. In this paper, the plant transfer functions G_{yu} and G_{yw} are derived after linearization and balanced

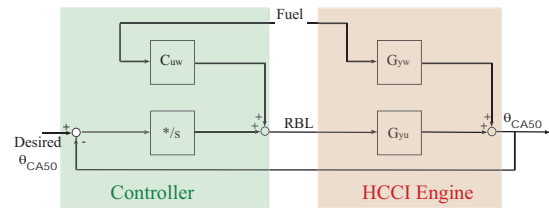


Fig. 7. Block diagram of the HCCI engine plant with a dynamic (cancellation) feedforward controller and an integral feedback controller.

realization are applied to the normalized full order model. The resulting feedforward C_{uw} is a fifth-order controller:

$$C_{uw} = \frac{-0.06s^5 - 4.56s^4 - 312.3s^3 - 3975s^2 - 6105s - 2338}{s^5 + 63.69s^4 + 1324s^3 + 9762s^2 + 14030s + 5354}. \quad (18)$$

The RBL command is augmented by an integral controller to avoid steady state θ_{CA50} errors:

$$RBL = C_{uw}(s) \cdot Fuel - \frac{0.1}{s} \cdot (\theta_{CA50}^{des} - \theta_{CA50}). \quad (19)$$

Fig. 8 shows the controlled performance with a static feedforward RBL controller and the dynamic feedforward RBL controller of (19) during fuel steps from 9-11-9 mg/cycle (2.4-3-2.4 bar imep) at 1000 rpm. Both the static and dynamic feedforward RBL controllers are able to regulate the steady-state IVC temperature T_{ivc} to the optimum equilibrium point on each steady-state temperature curve, thus regulating the combustion timing during the fuel step changes. However, the transient IVC temperature excursions are bigger during the instantaneous step change in RBL commanded by the static feedforward controller as shown in Fig. 8. On the other hand, with tighter regulation of T_{ivc} , the dynamic feedforward controller improves the combustion timing regulation during transients.

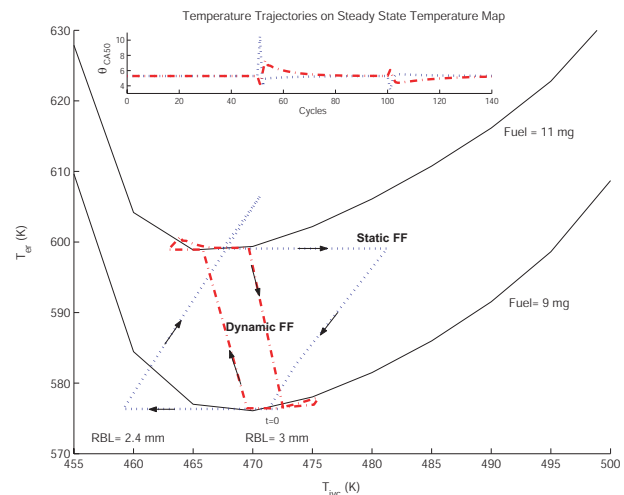


Fig. 8. Temperature trajectories and combustion timing with static and dynamic feedforward RBL controllers for fuel steps 9→11 mg/cycle and 11→9 mg/cycle.

During larger fuel step changes 9-16-9 mg/cycle (2.4-4.5-2.4 bar imep) at 1000 rpm, however, both the static

and dynamic feedforward controllers fail to make successful transitions. The dynamic feedforward controller is derived from the linearized plant and does not take into account the nonlinear temperature dynamics. Fig. 9 shows that the linear dynamic feedforward controller is not able to stabilize the temperature dynamics due to the change of sign on the nonlinear curve during large fuel steps. On the other hand, the static feedforward controller captures the system nonlinearity algebraically but not the system dynamics. First, as shown in Fig. 9, while fueling level increases from 9 to 16 mg/cycle, the static feedforward controller causes a large temperature excursion and thus unhealthy combustion timing. When fuel increases, the static feedforward controller issues a command to decrease RBL immediately. During the simultaneous decrease in RBL, extremely late combustion or misfire occurs due to the dramatic drop in T_{ivc} . Second, the engine temperature grows unbounded when fuel steps down from 16 to 9 mg/cycle. When fuel steps down, the static feedforward controller causes RBL to increase immediately, bringing into the cylinder a large amount of hot exhaust gas that was produced in the previous cycle by the high fueling level (16 mg/cycle). The hot charge advances the combustion timing, causing the exhaust gas to become even hotter, which further advances the timing in the subsequent cycle. As can be seen in Fig. 9, the hot charge brings the temperature trajectory to the unstable region, as we discussed in Sec. IV. Therefore, for applications that require large load transitions, a gain scheduling linear controller or a nonlinear controller such as the one in [12] may be necessary to stabilize the thermal dynamics.

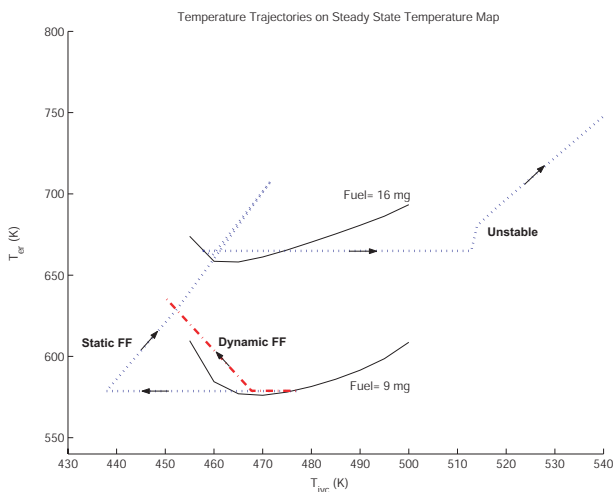


Fig. 9. Temperature trajectories with static and dynamic feedforward RBL controllers for fuel steps 9→16 mg/cycle and 16→9 mg/cycle.

VI. CONCLUSION

The existence of multiple steady state temperature equilibria and their stability under different heat transfer conditions is analyzed in this chapter. The results indicate that the wall temperature and heat management are very important to the operation of HCCI engines. Heat management in the exhaust

runners is especially important when a variable exhaust valve actuation (rebreathing) is used. We show that heat transfer in the exhaust runners can change the temperature of the reinducted exhaust gas and thus change the slope of the breathing temperature curve and affect the system stability. It is also shown that the autoignition, which is based on high exhaust gas recirculation and thus strong cycle-to-cycle temperature coupling, can depart from the region of attraction of a stable equilibrium during large and fast changes in fueling level. The linear dynamic feedforward controller and static feedforward controller, both of which are able to make successful small load transitions, fail to make large load transitions between an extremely hot region (higher fueling level) and a cooler region (lower fueling level). Similar difficulties are expected for mode transition from SI to HCCI [13] or from CI to HCCI [14].

ACKNOWLEDGMENT

This work is funded by Department of Energy under contract DE-FG02-06CH11300. We thank General Motors Corporation for the experimental data.

REFERENCES

- [1] P. Najt and D. Foster, "Compression-ignited homogeneous charge combustion," *SAE paper 830264*.
- [2] R. H. Thring, "Homogeneous-charge compression-ignition (HCCI) engines," *SAE paper 892068*.
- [3] C. J. Chiang and A. G. Stefanopoulou, "Sensitivity analysis of combustion timing and duration of homogeneous charge compression ignition (HCCI) engines," in *Proc. of the American Control Conf.*, 2006, pp. 1857–1862.
- [4] D. S. Stanglmaier and E. Roberts, "Homogenous charge compression ignition (HCCI): Benefits, compromises, and future engine applications," *SAE paper 1999-01-3682*.
- [5] J. Martinez-Frias, S. M. Aceves, D. Flowers, J. R. Smith, and R. Dibble, "HCCI control by thermal management," *SAE paper 2000-01-2869*.
- [6] D. J. Rausen, A. G. Stefanopoulou, J.-M. Kang, J. A. Eng, and T.-W. Kuo, "A mean-value model for control of homogeneous charge compression ignition (HCCI) engines," *ASME Journal of Dynamic Systems, Measurement and Control*, vol. 127, no. 3, pp. 355–362, 2005.
- [7] G. Shaver, J. Gerdes, P. Jain, P. Caton, and C. Edwards, "Dynamic modeling of residual-affected hcci engines with variable valve actuation," *ASME Journal of Dynamic Systems, Measurement and Control*, vol. 127, no. 3, pp. 374–381, 2005.
- [8] C. J. Chiang and A. G. Stefanopoulou, "Steady-state multiplicity and stability of thermal equilibria in homogeneous charge compression ignition (HCCI) engines," in *43rd IEEE Conference on Decision and Control*, vol. 2, 2004, pp. 1676–1681.
- [9] J. O. Olsson, P. Tunestal, B. Johansson, S. Fiveland, R. Agama, M. Willi, and D. Assanis, "Compression ratio influence on maximum load of a natural gas fueled HCCI engine," *SAE paper 2002-01-0111*.
- [10] J. B. Heywood, *Internal Combustion Engine Fundamentals*. McGraw-Hill Inc, 1988.
- [11] C. J. Chiang and A. G. Stefanopoulou, "Control of thermal ignition in gasoline engines," in *Proc. of the American Control Conf.*, 2005, pp. 3847–3852.
- [12] C. J. Chiang, A. G. Stefanopoulou, and M. Janković, "Nonlinear observer-based control of load transitions in homogeneous charge compression ignition (HCCI) engines," *IEEE Transactions on Control Systems Technology (Special Issue on Control Applications in Automotive Engineering)*, May 2007.
- [13] H. Santoso, J. Matthews, and W. K. Cheng, "Managing SI/HCCI dual-mode engine operation," *SAE paper 2005-01-0162*.
- [14] C. Musardo, B. Staccia, M. Shawn, Y. Guezennec, and G. Rizzoni, "Supervisory control for nox reduction of an HEV with a mixed-mode HCCI/CIDI engine," in *Proc. of the American Control Conf.*, 2005, pp. 3877–3881.